1

Bioinspired Polydopamine and Composites for Biomedical Applications

Ziyauddin Khan[1], Ravi Shanker[1], Dooseung Um[1], Amit Jaiswal[2], and Hyunhyub Ko[1]

[1] *Ulsan National Institute of Science and Technology (UNIST), School of Energy & Chemical Engineering, UNIST-gil 50, Ulsan 44919, Republic of Korea*
[2] *BioX centre, School of Basic Sciences, Indian Institute of Technology Mandi, Kamand, Mandi 175005, Himachal Pradesh, India*

1.1 Introduction

Understanding the systems and functions existing in nature and mimicking them led researchers to discover novel materials and systems useful in all disciplines of science, whether it is chemistry, biology, electronics, or materials science [1, 2]. Numerous biopolymers (carbohydrates and proteins) such as cellulose, starch, collagen, casein, and so on, are naturally occurring polymers and have vast application in the biomedical research field. In recent years, PDA, a bioinspired polymer having a molecular structure similar to that of 3,4-dihydroxy-L-phenylalanine (DOPA), which is a naturally occurring chemical in mussels responsible for their strong adhesion to various substrates, has been regarded as a promising polymer, with applications in energy, electronics, and biomedical fields, due to its chemical, optical, electrical, and magnetic properties [3, 4]. For example, PDA can be easily deposited or coated with any substrate type of one's choice, including superhydrophobic surfaces, making it a highly beneficial material for coating and strong adhesive applications [3]. PDA also has various functional groups such as amine, imine, and catechol in its structure, which opens up the possibility for it to be integrated covalently with different molecules and various transition metal ions, thus making it a prerequisite in many bio-related applications.

Herein, this chapter describes the general synthetic route, polymerization mechanism, key properties, and biomedical applications of PDA. PDA can be synthesized by oxidation and self-polymerization of dopamine under ambient conditions; however, it can also be synthesized by enzymatic oxidation and electropolymerization processes, which are discussed in detail. Furthermore, this chapter also gives a brief idea about the characteristic properties of PDA such as optical, electrical, adhesive, and so on, followed by an extensive discussion of its applications in drug delivery, bioimaging, tissue engineering, cell adhesion and proliferation, and so on, with a special focus on its conductivity.

Electrically Conductive Polymers and Polymer Composites: From Synthesis to Biomedical Applications, First Edition. Edited by Anish Khan, Mohammad Jawaid, Aftab Aslam Parwaz Khan, and Abdullah M. Asiri.

1.2 Synthesis of Polydopamine

1.2.1 Polymerization of Polydopamine

In the general synthesis of PDA, the dopamine monomer undergoes oxidation and self-polymerization in an alkaline medium (pH > 7.5) with air as an oxygen source for oxidation. This self-polymerization of the oxidative product of dopamine reaction is extremely facile and does not require any complicated steps. Although the polymerization of dopamine looks simple, the synthesis mechanism has not yet been investigated comprehensively [3, 5]. As shown in Figure 1.1, it is believed that in an alkaline solution dopamine is first oxidized by oxygen to dopamine quinone, followed by intramolecular cyclization to leucodopaminechrome through Michael addition. The formed intermediate leucodopaminechrome undergoes further oxidation and rearrangement to form 5,6-dihydroxyindole, which may yield 5,6-indolequinone by further oxidation [6]. Both these indole derivatives can undergo branching reactions at a different position (2, 3, 4, and 7), which can yield various isomers of dimers and finally higher oligomers. These oligomers can self-assemble by dismutation reaction between catechol and *o*-quinone to form a cross-linked polymer [3, 6]. Furthermore, there have been various other reports in which the authors have tried to investigate the exact mechanism of PDA formation, but this aspect is still unclear [7–10].

Along with the oxidation and self-polymerization of dopamine in an alkali solution, PDA can also be synthesized by enzymatic oxidation and electropolymerization processes [11–13]. Enzymatic polymerization has attracted considerable interest owing to its environment-friendly characteristics. Inspired by the formation of melanin in a living organism, dopamine has been enzymatically polymerized using laccase enzyme into PDA at pH 6 (Figure 1.2) [1]. In laccase-catalyzed polymerization, laccase gets entrapped into the PDA matrix, which offers great advantages in biosensing and biofuel cell applications. In contrast to the enzymatic process, dopamine can also be electropolymerized and deposited

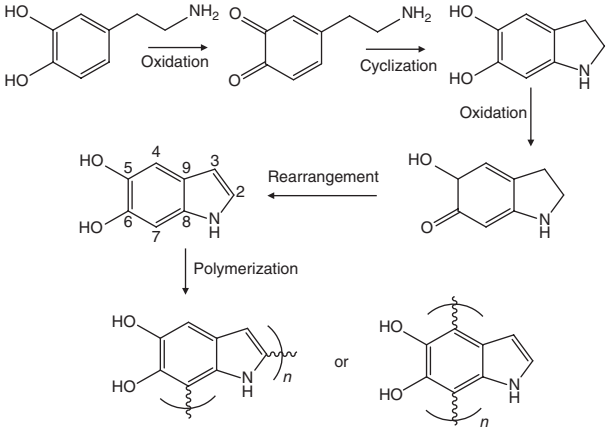

Figure 1.1 Formation mechanism of PDA in an alkali solution. (Reprinted with permission from Refs [5] and [3] Copyright 2011 and 2014 American Chemical Society.)

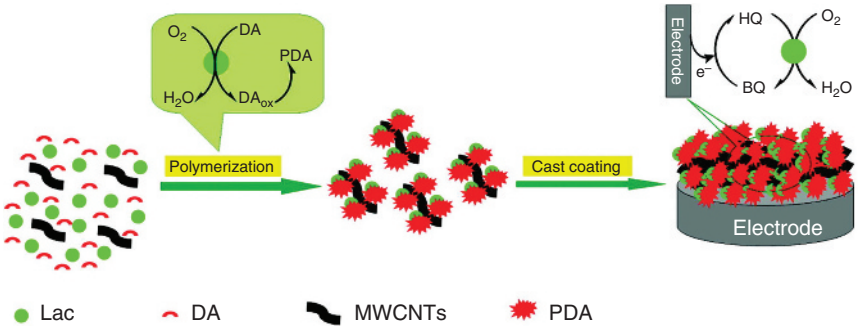

Figure 1.2 Graphical representation of the formation of PDA–laccase–MWCNT nanocomposite film on GCE for hydroquinone biosensing. (Reprinted with permission from Ref. [1] Copyright 2010 American Chemical Society.)

on the substrate at a given potential in a deoxygenated solution. However, the electropolymerization process requires highly conductive materials, which is one of the main disadvantages of this process of dopamine polymerization.

1.2.2 Synthesis of Polydopamine Nanostructures

A great deal of attention has been paid of late toward the synthesis of monodisperse PDA nanoparticles and PDAs with different morphologies, which can be used for other applications such as chemical sensors, energy storage, and so on. The size of the PDA particles can be tuned using a different ratio of solvents and base [14, 15]. Usually, after the self-polymerization reaction, PDA tends to form uniform spherical particles after prolonged reaction up to 30 h. Ai *et al.* have demonstrated that the size of PDA spheres can be controlled by varying the ratio of ammonia to dopamine and thereby synthesize various sizes of PDA nanoparticles (Figure 1.3a–e) [14]. In another study, Jiang *et al.* reported that varying the amount of ethanol and ammonia can also tune the size of PDA particles (Figure 1.3f) [15].

Recently, PDA with some unique morphology, for example, PDA nanotubes, have also been reported using a template-based method. Yan *et al.* coated a PDA layer on ZnO nanorods as a template by self-polymerization reaction of dopamine; and later the ZnO nanorod template was etched by ammonium chloride solution, leaving behind hollow PDA nanotubes (Figure 1.4a) [16]. Xue *et al.* reported the scalable synthesis of PDA nanotubes using curcumin crystal as a template [17], as shown in Figure 1.4b. These PDA nanotubes are several tens of micrometers long with 40-nm wall thickness and 200- to 400-nm tube diameter, which can be tuned by stirring rate and curcumin crystal size. Further to nanotubes, freestanding films of PDA and hybrid PDA films have also been prepared for their use in structural color, by layer-by-layer assembly [18–20]. In one of the reports, Yang *et al.* have reported composite freestanding films of PDA with polyethyleneimine (PEI), which was grown on air/water interface [20]. The prepared film was a freestanding transparent film, more than 1 cm in diameter, 80 nm in thickness, and without any visual defects on the film surface as proved by field

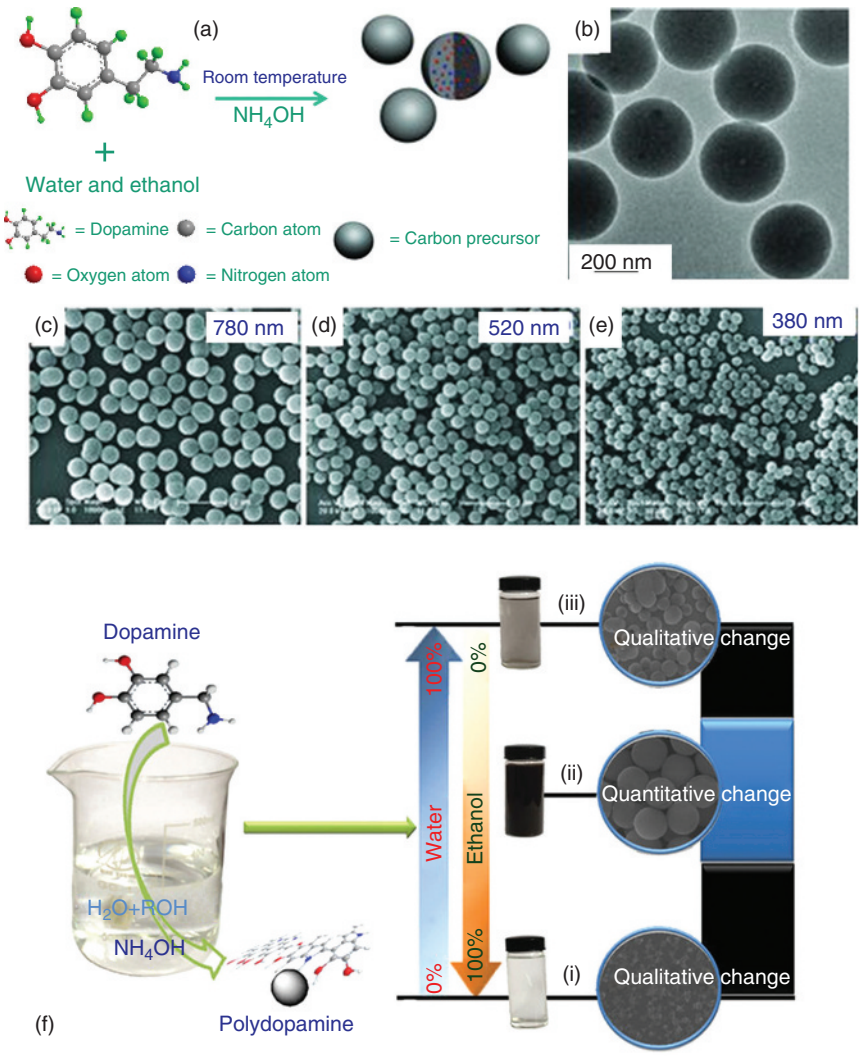

Figure 1.3 (a–e) Schematic representation of sub-micron size PDA particles and their morphological study. (Redrawn and reprinted with permission from Ref. [14] Copyright 2013 Wiley-VCH.) (f) Study of EtOH and ammonia concentration on PDA morphology. (Redrawn and reprinted with permission from Ref. [15] Copyright 2014 Nature Publishing Group.)

emission scanning electron microscopy (FESEM). The film size can be tuned by the container which holds the dopamine and PEI solution.

Although there has been excellent progress in preparing different shapes and sizes of PDA nanoparticles, producing monodisperse nanoparticles is still a challenge, which is an essential parameter in biological science to ensure consistency in experiments. In the near future we can expect that this field will make further progress in producing highly monodisperse nanoparticles.

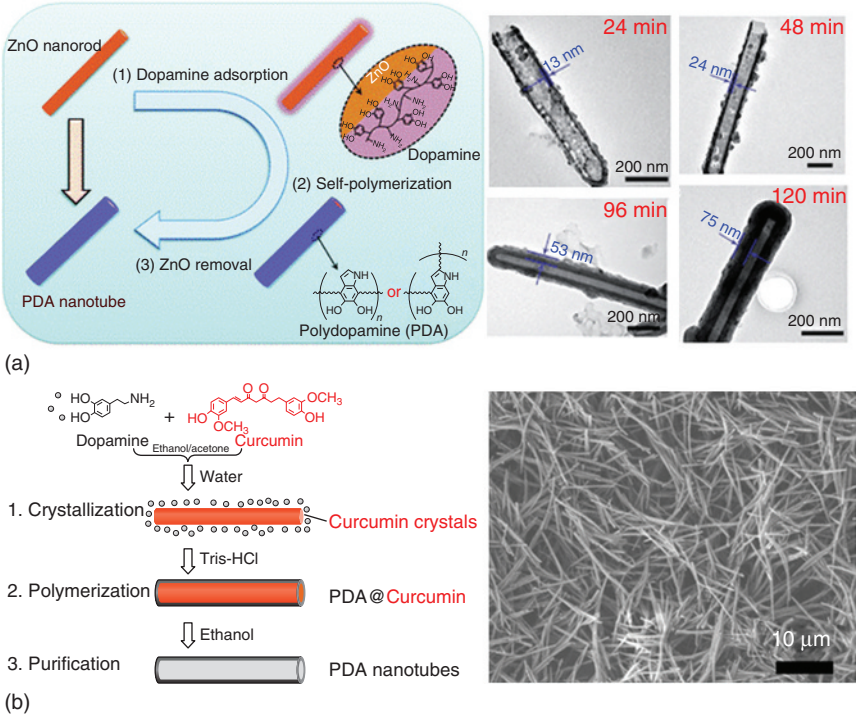

Figure 1.4 (a) Graphical representation of PDA nanotube synthesis and its high-resolution TEM images. (Reprinted with permission from Ref. [16] Copyright 2016 Royal Society of Chemistry.) (b) PDA nanotube synthesis by curcumin crystals and its morphology. (Reprinted with permission from Ref. [17] Copyright 2016 American Chemical Society.)

1.3 Properties of Polydopamine

1.3.1 General Properties of Polydopamine

PDA is an analog of eumelanin (a type of natural melanin) due to the similarity in chemical structure/component, which leads to the resemblance in physical properties [3, 21, 22]. Therefore, PDA has been regarded as a natural biopolymer, which has been utilized as a coating material in various applications. PDA is most commonly known for its inherent adhesive property; but functionalities of PDA have not been limited to adhesion as it possesses various properties, which are listed and discussed here.

1) *Optical properties*: PDA shows broadband absorption ranging from ultraviolet (UV) to visible region, which increases exponentially toward the UV spectrum as in the case of the naturally occurring analog eumelanin. The absorption in the UV region originates from oxidation of dopamine to dopachrome and dopaindole; however, the absorption in the visible and near-infrared (NIR) region is due to the subsequent self-polymerization process [23, 24].

2) *Electrical conductivity*: In 1974, McGinness *et al*. observed the electrical switching properties of eumelanin, and since then it was assumed that eumelanin has organic semiconductive properties [25, 26]. It was suggested that highest occupied molecular orbital (HOMO) and lowest occupied molecular orbital (LUMO) levels of eumelanin act as valence and conduction bands as in the case of the semiconductor. Eumelanin is an aromatic compound that results in HOMO and LUMO levels composed of π-system and the charges move through this π-system, leading to the electrical conductivity of eumelanin. See the electrical properties (Section 1.3.2) for a detailed description.
3) *Adhesive property*: PDA displays a strong adhesive property to all kinds of surfaces and it is believed that this property arises due to the presence of the catechol group. However, it is not well understood yet how PDA diffuses to a different kind of surface, but based on literature it can be stated that PDA interacts with the substrate by a covalent or noncovalent binding mechanism [27, 28].
4) *Biocompatibility and biodegradation property*: Biocompatibility and biodegradation are the key parameters for any material to have an application in the biomedical field. PDA, a major component of melanin, shows exceptional biocompatibility even at high doses when its cytotoxicity was studied with mouse 4T1 breast cancer cells and human cervical cancer cells (HeLa cells) [29]. However, melanin can be degraded *in vitro* in the presence of oxidizing agents such as hydrogen peroxide, which is also the case for PDA [30]. The color fading was observed in PDA when incubated with hydrogen peroxide, which suggests its degradation [29]. Bettinger *et al*. in an *in vivo* study also suggests complete degradation of implanted PDA in 8 weeks [31].

1.3.2 Electrical Properties of Polydopamine

Organic semiconductors possess structural similarity to biological compounds, which opens up the possibility of their use in biomedical science [32]. A few of the most used organic semiconductors in biomedical science are poly(3,4-ethylenedioxythiophene):poly(4-styrenesulphonate) (PEDOT:PSS) and poly(3-hexylthiophene) (P3HT) due their excellent ion and electron mobility, and higher tissue integration ability [33, 34]. PEDOT:PSS is one of the first and widely used active channels in biomedical devices such as organic electrochemical transistors (OECTs) [33]. The performance of these devices can be improved by making a thinner film of the active channel below 100 nm [35, 36]. However, past literatures for such devices are mainly based on four transducing materials: P3HT, polypyrrole, PEDOT:PSS, and polyaniline [37]. This opens up the possibility of searching for alternative materials to be used in bioelectronic devices, in particular for edible electronics.

Interest in melanin, both natural and synthetic, has bloomed since the seminal study by McGinness *et al*. [25]. In recent years, PDA, also called synthetic melanin similar to natural melanin, has emerged as an additional candidate to be used in bioelectronics for transduction purposes. Since major research work in the context of the conductivity studies has been done on natural melanin, from

hereon we use the word melanin as PDA's properties are essentially similar to those of melanin. Melanin has some very interesting properties for biomedical application, such as broad monotonic optical absorption [38, 39], free radical population state [24, 40], and the possibility of making thin films less than 100 nm, thus offering device integration with neurons [4, 24, 41], hydration-dependent electrical and photoconductivity ranging from 10^{-8} to $10^{-4}\,S\,cm^{-1}$, depending on the hydrated state [39, 42], and the ability to link electronic and protonic/ionic signals in a common mechanism through comproportionation reaction (CRR) [43].

To describe each point is beyond the scope of this chapter, so we have mainly focused on its charge transport/electrical properties based on two different charge transport models available in the literature. Of the two models available to explain melanin charge transport properties, the first is based on an amorphous semiconductor model (ASM) and the other is hydration-dependent muon spin resonance (μSR) described by a CRR.

1.3.2.1 Amorphous Semiconductor Model (ASM) of Melanin Conductivity

This model is based on the four observations and considers melanin to be an amorphous semiconductor because it shows the following:

- Semiconductor-type Arrhenius temperature dependence on its conductivity [42, 44]
- Bistable switching behavior [25, 45]
- Broadband optical absorbance [39]
- Stable free radical: unpaired electrons at the Fermi energy level [46].

However, there are a few shortcomings in this model, the first one being its broad absorbance (Figure 1.5a), which can also be described by the oligomer structure, that is, the spectrum is made up of multiple individual chemical chromophores [39, 49]. It cannot describe the delocalized electronic state for which large 2D sheet-type structures are required; this is not true for oligomers, which are fairly small. The second is that only wet melanin samples display hydration-dependent switching behavior.

To observe the conductivity of hydration-dependent melanin, Mostert *et al*. measured the water–melanin adsorption isotherm on melanin pallet samples and the result is shown in Figure 1.5b, which exhibits the significant presence of water in melanin [47]. Mostert *et al*. also measured the hydration-dependent conductivity using two different contact geometries, that is, sandwich and van der Pauw, and the results are shown in Figure 1.5c,d [48].

It can be seen from Figure 1.5c that the conductivity increases by orders of magnitude in a sub-exponential manner. However, the specimen was found to be at nonequilibrium in sandwich geometry due to low exposure of the surface area by the presence of the contacts. Therefore, an open-contact arrangement, van der Pauw geometry (Figure 1.5d inset), has been used where ~71% of surface area can be exposed than to ~37% in sandwich geometry; and the result is shown in Figure 1.5d [48]. Interestingly, these data were found not to be in agreement with previous literature and also could not be explained by the existing ASM theory [42, 50].

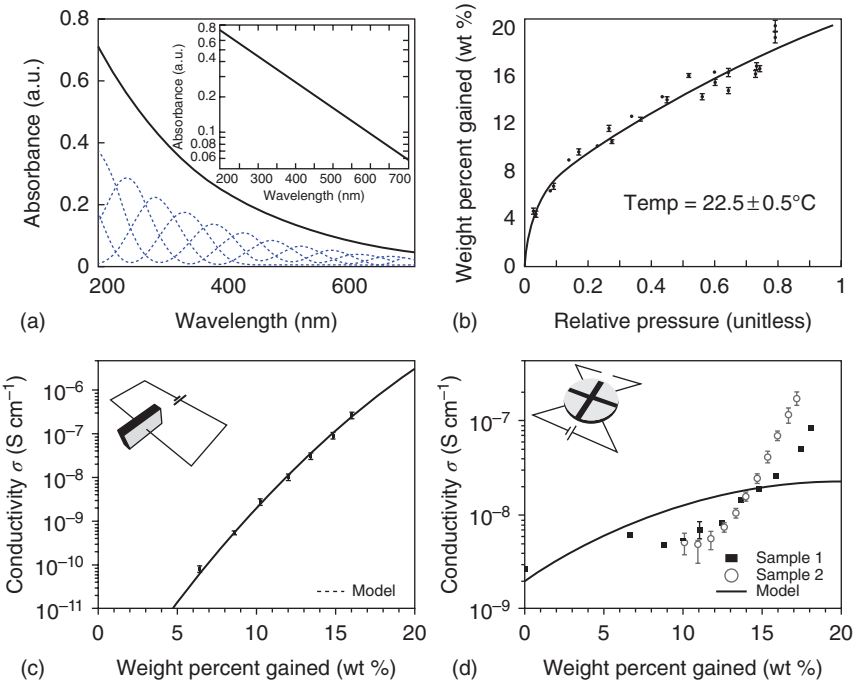

Figure 1.5 (a) Melanin broadband optical absorbance spectrum (inset for log linear axes) and peaks below show individual absorbance peak chromophores. (Reprinted with permission from Ref. [39] Copyright 2005 Royal Society of Chemistry.) (b) Equilibrium adsorption isotherm for melanin in the presence of water vapor. (Reprinted with permission from Ref. [47] Copyright 2010 American Chemical Society.) (c) Melanin dark conductivity versus water content in sandwich geometry. (d) Melanin dark conductivity versus water in van der Pauw geometry. ((c and d) Reprinted with permission from Ref. [48] Copyright 2012, AIP Publishing LLC.)

This argument was also supported with controlled photoconductivity experiments, which are shown in Figure 1.6a–d and have a simple explanation: as heating increases, water desorption takes place and produces a negative conductivity, whereas as per ASM it is due to the trap states in the photo bandgap of melanin [48]. This study also shows strong evidence that water plays a crucial role in the basic charge transport mechanism and ASM cannot be applied to melanin.

1.3.2.2 Spin Muon Resonance Model (SMRM) of Melanin Conductivity

To further elucidate the charge transport mechanism of melanin, an alternative technique – magnetic resonance (μSR) – has been used because it can discount electrical effects, probe the material's local environment and mobility behavior of protons in the specimen [51], and estimate the number density of the free radicals [52, 53]. μSR demonstrates that in melanin, charge transport is determined by an equilibrium reaction. The controlled, water-dependent μSR carried out as a function of hydration is shown in Figure 1.7. It can be seen from Figure 1.7a that muon hopping rate ν does not change throughout the hydration range of

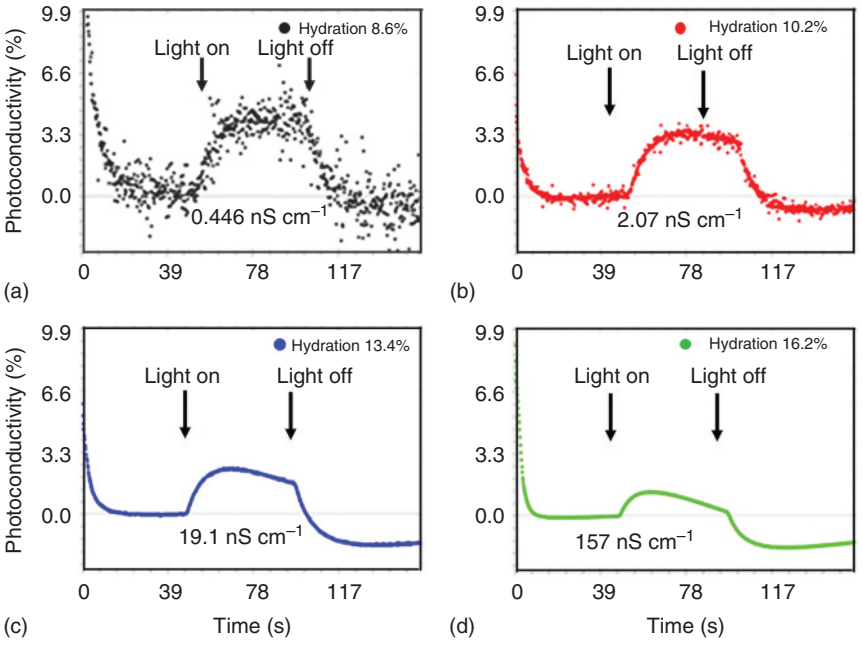

Figure 1.6 Melanin photoconductivity versus time for four different hydration levels: (a) 8.6%, (b) 10.2%, (c) 13.4%, and (d) 16.2%, under dark, illuminated, and dark sequence each for 50 s. (Reprinted with permission from Ref. [48] Copyright 2012, AIP Publishing LLC.)

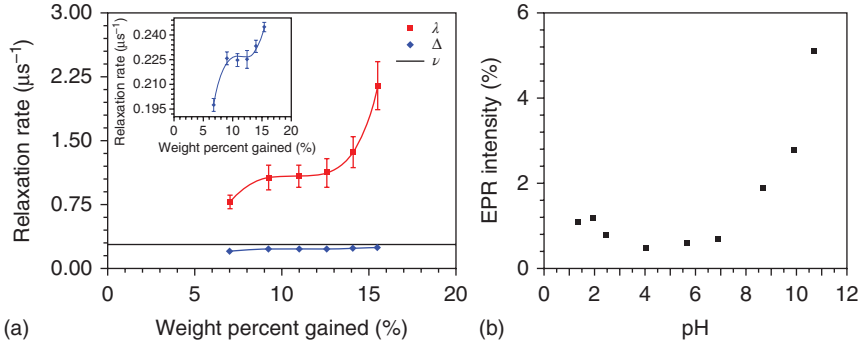

Figure 1.7 (a) The μSR relaxation data obtained on hydrated melanin pellets. (b) A pH-dependent titration EPR study for colloidal suspensions of melanin. (Reprinted with permission from Ref. [54] Copyright 2012, PNAS.)

melanin, meaning that proton mobility remains the same. However, muon relaxation Δ and spin–lattice relaxation rate λ show qualitative changes and exhibit a response similar to the conductivity data in Figure 1.5d because λ is directly related to free-radical density in a sample; thus, the unpaired electrons present in melanin increase with hydration, along with the conductivity. Mostert *et al.* suggested that a CRR, which is essentially an equilibrium reaction, can only explain the conductivity and μSR results [55].

In CRR, two different oxidative state chemical units of melanin form semiquinones, which are hydronium and free radicals on the introduction of water (Eq. (1.1)) [54]. With the increase of hydration, an imbalance occurs between the reactant and product; and to counterbalance this, the unevenness reaction starts producing more products in accordance with Le Chatelier's principle [54, 55]. In addition, it was also explained by electron paramagnetic resonance (EPR) measurement, as shown in Figure 1.6b, that when the base is added (the same effect as adding water), the titration curve displays a response similar to both the μSR and conductivity [54]. Therefore, it was proposed that the conductivity increase in charge carrier density, both protonic as well as electronic, is due to the link between two charge entities and which makes melanin a potential transducing material for biomedical devices.

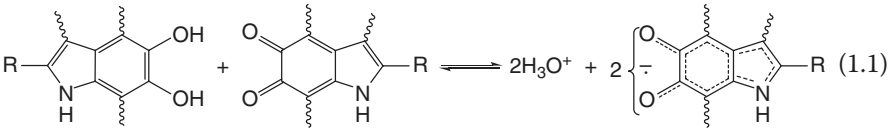

(1.1)

1.4 Applications of Polydopamine

As mentioned, PDA has a range of intriguing properties and is a potential candidate in a variety of important applications, from biomedical science to energy, as shown in Figure 1.8. For example, in energy and environment applications,

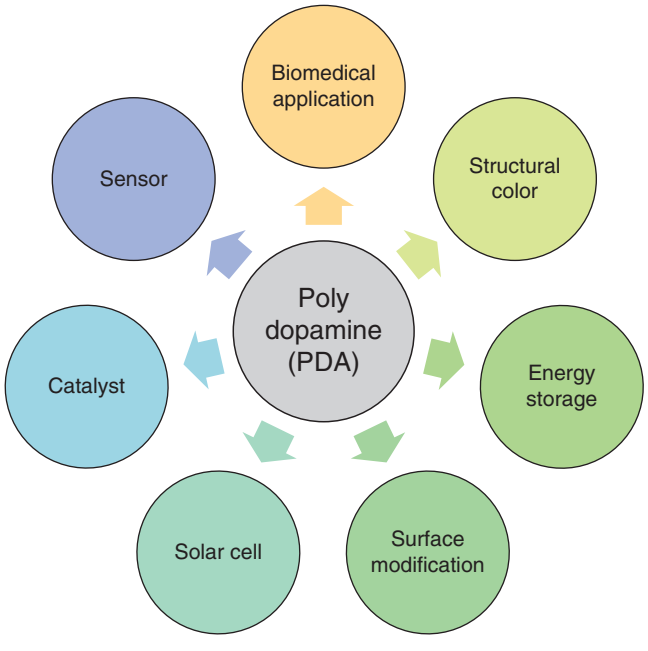

Figure 1.8 Application of polydopamine in various emerging research fields.

heterogeneous photocatalysis, which is known as a cost-effective approach for dye degradation and solar water splitting under light irradiation [56–60], PDA can be coupled with photocatalytic materials which help the photocatalytic materials improve their performance synergistically by π–π^* electronic transition [61]. Feng *et al.* synthesized core–shell AgNPs@PDA and used it for photocatalytic degradation of neutral red dye. They reported that the AgNPs@PDA catalyst showed improved performance than bare Ag NPs and PDA under UV irradiation. PDA can produce holes under UV illumination, which extends the duration of the recombination rate of photogenerated charge carrier and results in enhancement in the lifetime of electron pairs due to the existence of π–π^* electronic transition. In addition, it also offers extra surface for dye adsorption. Recently, Mao *et al.* synthesized TiO_2@PDA photocatalyst and used it for the degradation of rhodamine B (RhB) under visible light illumination [62]. TiO_2 is a well-known UV-light-driven photocatalyst; however, PDA shows strong absorption in the visible region, and coupling of these two can form a catalyst which can have visible light activity, as investigated by Mao *et al.* The authors have coated different thickness PDA on TiO_2 nanoparticles and found that 1 nm coated PDA on TiO_2 showed highly improved performance for RhB degradation. The reason for such an enhancement is still not clear, but it was proposed theoretically by Persson and coworkers that there is a one-step charge transfer from dopamine to the conduction band of TiO_2, which can improve the catalytic performance of the composite material. Besides, PDA can be utilized for various energy-related applications such as batteries, supercapacitors, and dye-sensitized solar cells [63–65]. However, as per the demand of the chapter, we mainly focus on its biomedical applications.

1.4.1 Biomedical Applications of Polydopamine

PDA, a major component of naturally occurring melanin, has vast biomedical application due to its exceptional biocompatibility, hydrophilicity, and thermal and adhesive properties. It can also undergo further reaction with various molecules/materials and produce hybrid materials with applications in diverse research fields. This section deals with the various biomedical applications of PDA and PDA-derived materials.

1.4.1.1 Drug Delivery

PDA capsules have been considered fascinating material for drug delivery owing to their high water solubility, exceptional biocompatibility, and biodegradation ability. The interest in the synthesis of PDA capsules with well-defined structures has increased tremendously for drug delivery because drugs can easily be encapsulated in the capsule's cavities. Various soft and hard template-based methods have been used to synthesize PDA capsules. However, the hard template method is least favored due to its requirement of harsh conditions for removal, which can hinder its application in the biomedical field [66–69]. The drug loading behavior of PDA capsules depends on the size of the capsules, as bigger capsule size increases the interior volume which leads to higher drug loading. Furthermore, the pH of the solution and the charge state of the loading molecules also greatly

affect the drug loading behavior [66, 70]. PDA have different functional groups and therefore display zwitterionic property. At low pH (pH ~ 3), the PDA capsule walls were positively charged; however, if the loading molecule is methyl orange (MO), which is in a neutral state at this pH, the presence of the sulfonate group gives it an anionic character. Thus, there exists strong ionic interaction between the positively charged PDA capsule and the negatively charged MO dye, which leads to higher loading of a dye molecule in PDA capsules. However, if the loading molecule is rhodamine 6G, then there is almost negligible loading of the dye molecule to PDA capsules because of strong electrostatic repulsion between the positively charged PDA and the positively charged rhodamine 6G at this pH [66]. Regardless of the high loading of the desired drug, these systems suffer from poor drug delivery in aqueous media which needs to be overcome [3].

1.4.1.2 Tissue Engineering

Tissue engineering has been considered an effective technique to replace damaged or diseased body parts with man-made artificial tissues or organs without any transmission disease. The research, in tissue engineering, is mainly focused on the development of effective scaffolds for cells and tissue growth [71]. Typically, in extracellular matrix cell attachment, proliferation and differentiation take place for natural tissues; and, therefore, it would be a prerequisite for effective tissue engineering that artificial scaffolds should be chemically and physically analogous to the extracellular matrix. Mesoporous SiO_2 has been used as scaffolds for tissue engineering because the big pores are beneficial to cell growth, while the mesoporous structure can also help transport drugs that stimulate bone-forming cells. However, mesoporous SiO_2 suffers from poor cytocompatibility and mineralization rate [72]. Wu *et al.* took advantage of the adhesive and hydrophilic properties of PDA and used it as a surface modifier for mesoporous SiO_2 to study the mineralization and cytocompatibility for drug delivery and bone tissue engineering [72]. Investigation into the *in vitro* mineralization and proliferation of bone marrow stem cells (BMSCs) revealed that the PDA-modified SiO_2 scaffold displayed noteworthy apatite mineralization and also that attachment of BMSCs on PDA-modified SiO_2 had been increased (Figure 1.9a,b). It would be worthwhile to mention here that despite these efforts, the SiO_2-based scaffold suffers from *in vivo* degradation.

Ku and Park utilized nanofibers of biodegradable polymer polycaprolactone and deposited a thin layer of PDA on top to improve the cell affinity with polymeric nanofibers [73]. It was observed that the cell can attach, spread, and survive effectively on PDA-modified fibers. 3-(4,5-Dimethylthiazol-2-yl)-2,5-diphenyltetrazolium bromide (MTT) assay suggests that human umbilical vein endothelial cells (HUVECs) displayed fivefold enhancement in viability on PDA-modified nanofibers (Figure 1.9c–f). These investigations suggest that PDA can play a vital role in the design of artificial scaffolds in future in the tissue engineering area.

1.4.1.3 Antimicrobial Applications

The robust adhesion of PDA on various substrates makes it viable for fabrication of antimicrobial surfaces [74–76]. Xu *et al.* fabricated antibacterial cotton by

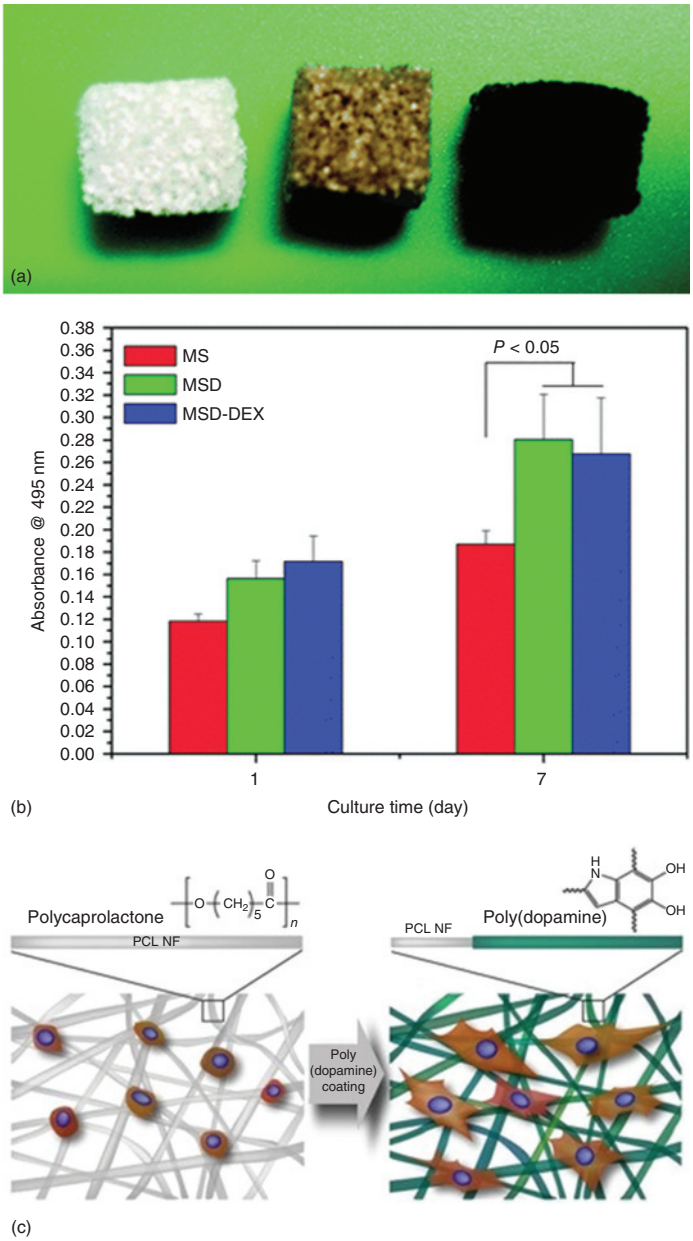

Figure 1.9 (a) Digital image of SiO_2 scaffold before and after 6- and 24-h modification with PDA; (b) the proliferation of BMSCs on mesoporous silica (MS), PDA-modified silica (MSD), and dexamethasone (DEX)-loaded MSD (MSD-DEX) scaffolds. MSD shows improved proliferation of BMSCs. (Reprinted with permission from Ref. [72], Copyright 2011 Royal Society of Chemistry.) (c) Cell adhesion graphics on PDA-coated polycaprolactone nanofibers (PCL NFs); (d) SEM image of fibers; (e) hydrophilicity measurement by contact angle analysis. (f) A number of live cells, and fold-increase of cell viability for HUVECs grown on unmodified, gelatin-coated, and PDA-coated PCL NFs. ((c–f) Reprinted with permission from Ref. [73], Copyright 2010 Elsevier Ltd.)

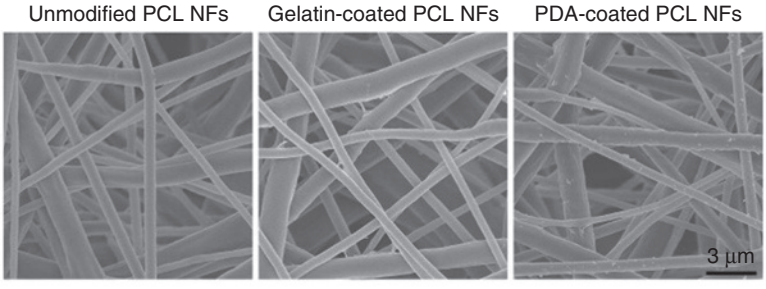

(d)

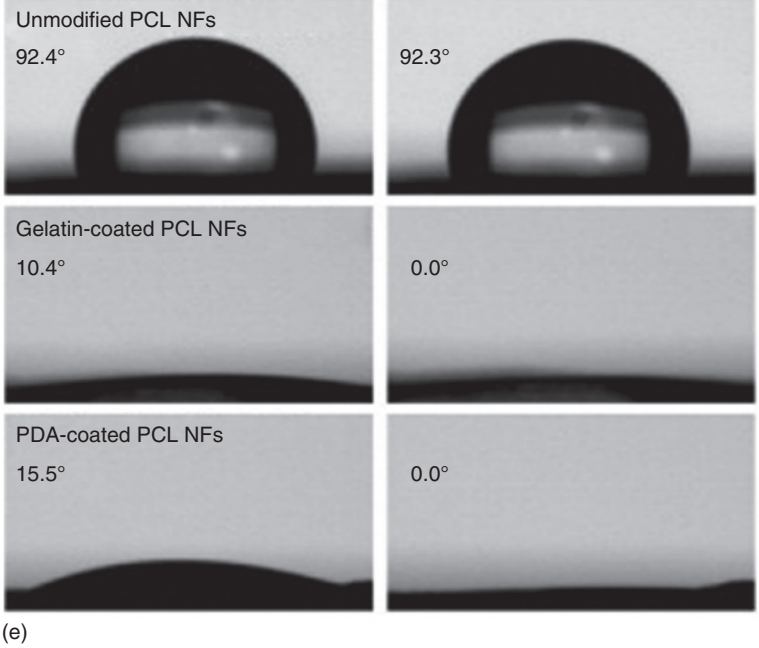

(e)

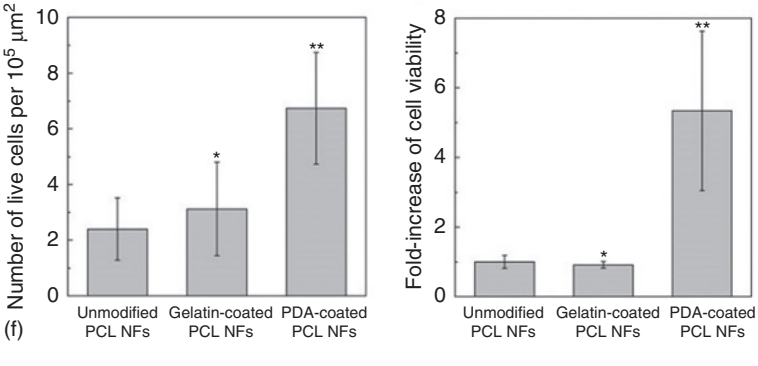

(f)

Figure 1.9 (*Continued*)

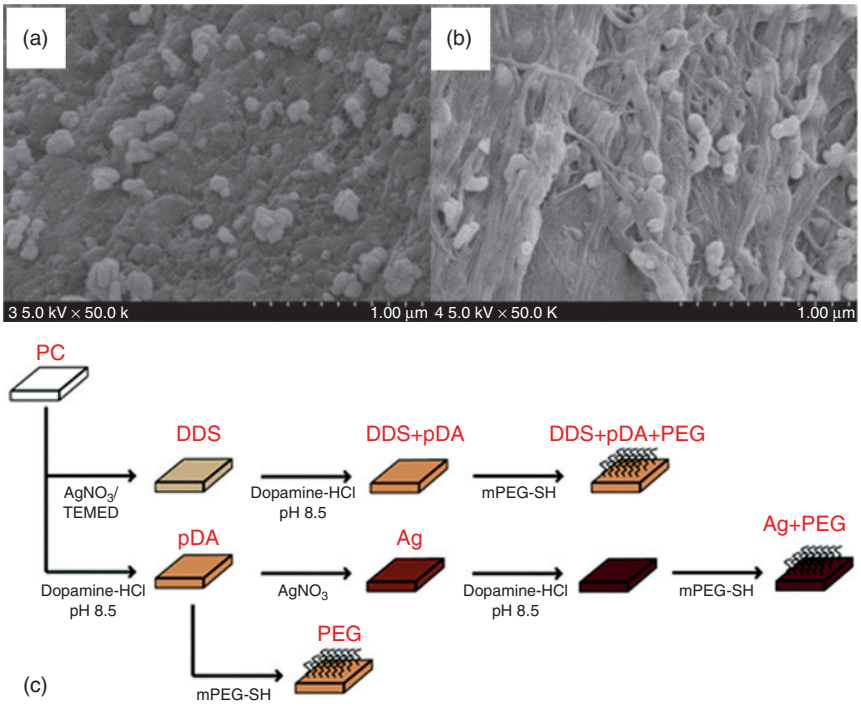

Figure 1.10 FESEM images of the dopa-cotton/AgNPs fabrics (a) unwashed and (b) after 30 washes. (Reprinted with permission from Ref. [74], Copyright 2011 Elsevier Ltd.) (c) Synthesis protocol of silver deposited (directly deposited silver (DDS)) and PDA-mediated antimicrobial coatings on a polycarbonate substrate. (Reprinted with permission from Ref. [75], Copyright 2011 American Chemical Society.)

coating a PDA layer on top of cotton fabrics, followed by *in situ* deposition of silver nanoparticles (Figure 1.10a) [74]. The prepared antibacterial cotton completely killed the bacteria. Even after 30 washes, the cotton fabrics were able to reduce 99.99% *Escherichia coli*, suggesting reusability and durability of cotton fabrics after coating with PDA (Figure 1.10b). Later, Sileika *et al.* utilized the adhesive property of PDA to make an antimicrobial surface by coating PDA on a polycarbonate substrate, followed by silver nanoparticle deposition as an antibacterial agent and *in situ* implanting of poly(ethylene glycol) (PEG) as an antifouling agent, as shown in Figure 1.10c [75]. The resulting substrate killed both gram-negative and gram-positive bacteria strains and resisted their attachment on the substrate. These outstanding studies reveal that PDA can provide a new avenue to fabricate an antibacterial substrate for use in practical applications.

1.4.1.4 Bioimaging

Fluorescence-based bioimaging of samples or cells has attracted tremendous attention in the past few decades with advances in nanotechnology and become the most widespread method in biomedical science due to its key properties, including high sensitivity, cost-effectiveness, and facile detection. Various kinds

of nanoparticles have been developed and are widely used as fluorescent probes for bioimaging of cells and tissues. An excellent review by Wolfbeis covers different nanoparticles widely used in probes for bioimaging such as doped silica, hydrogels, noble metal nanoparticles, quantum dots, carbon dots, upconversion nanoparticles, and so on [77, 78]. However, their cytotoxicity is still a debatable issue, as discussed by Zhang *et al.* [79]. As a recent addition to nanoparticle-based bioimaging, PDA has emerged as a new class of biocompatible organic fluorescent material. In a study, Wei and coworkers synthesized polydopamine fluorescent organic nanoparticles (PDA-FONs) and reported excitation-wavelength-dependent emission reaching maximum at 440 nm excitation with excellent photostability [80]. These PDA-FONs offer a simple fabrication method in contrast to the conventional method of complex organic synthesis of FONs (Figure 1.11). In addition, PDA has also been used as a coating material to enhance optical signals of fluorescent materials such as graphene quantum dots, and so on [81, 82]. Despite excellent biocompatibility, the fluorescence intensity is a rather weak point to overcome. Therefore, the future work will be on the design of novel PDA-based multifunctional fluorescent nanoparticles with tunable size, morphology, and fluorescent properties.

1.4.1.5 Cell Adhesion and Proliferation

Currently, interest in immobilization of cells by new synthetic materials is crucial to promote cell adhesion. PDA has emerged as a simple, versatile, and biocompatible material for such applications, which show excellent cellular response and strong affinity of cells to PDA coatings. PDA shows potential to enhance cell immobilization on various kinds of substrates. In a study, Yang *et al.* have shown that using PDA coating on living yeast cell can control and preserve cell division (Figure 1.12) [83]. Lee *et al.* observed PDA coating cytocompatibility is cell dependent and reported fibroblast and megakaryocytes cell adhesion to PDA-coated surfaces [4]. Park and coworkers reported excellent adhesion *in vitro* cytocompatibility of HUVECs on PDA-coated polycaprolactone nanofibers [73]. PDA coating also offers a key method to make bioactive surfaces including non-wetting and 3D porous scaffolds [84–86].

In addition to the excellent binding abilities, PDA-treated surfaces overcome the challenges of adhesive proteins for cellular patterning and can be deposited using different deposition methods such as microfluidic, micro-contact printing, and lithography (Figure 1.13 shows cell pattering using PDA ink) [4, 83, 87, 88]. In addition, combined studies on submicron topography and surface chemistry effect on cells have shown synergic enhancement in cell adhesion and proliferation [89, 90]. The possible mechanism of cell adhesion is also reported and is likely due to higher immobilization and/or adsorption of adhesive proteins [84, 85]. Recent studies suggest a new mechanism that the quinone group of PDA induced a larger amount of protein adsorption, and thus promoted endothelial attachment and proliferation [91–93].

1.4.1.6 Cancer Therapy

Photothermal therapy (PTT) is a minimally invasive treatment in which NIR light radiation is used for the treatment of many medical conditions such as

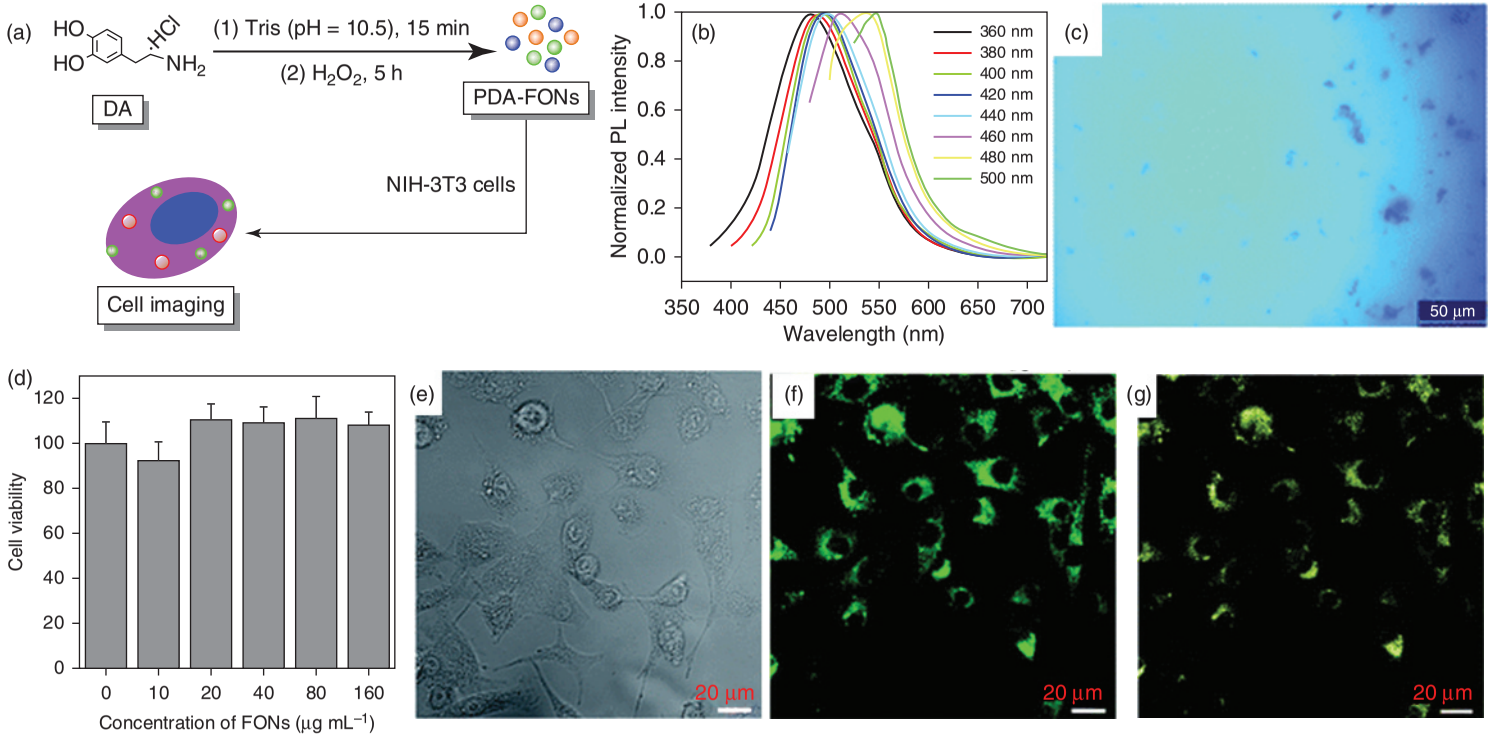

Figure 1.11 (a) Schematic illustration for the preparation of PDA-FONs and their application in cell imaging. (b) Normalized photoluminescence emission spectra of PDA-FON dispersion at different excitation wavelengths from 360 to 500 nm. (c) Fluorescence microscopy photograph of the PDA-FON dispersion excited by UV light (340–380 nm). (d) Effect of PDA-FONs on NIH-3T3 cells. (e–g) are confocal laser scanning microscopy images of cells imaged under bright field 405- and 458-nm excitations, respectively. (Reprinted with permission from Ref. [80] Copyright 2012 Royal Society of Chemistry.)

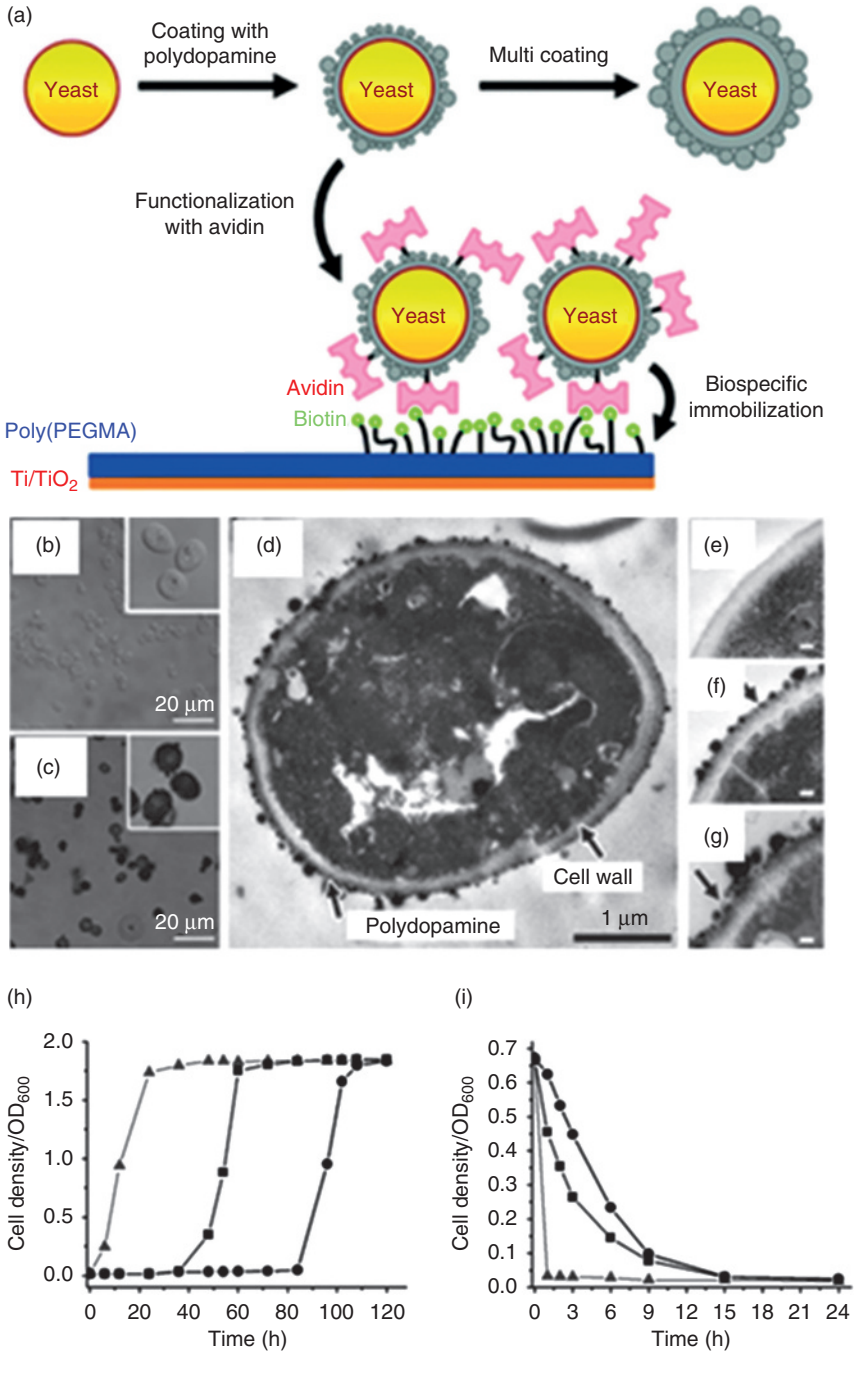

Figure 1.12 (a) Schematic of the PDA and its encapsulation and surface functionalization on yeast cells. Confocal micrographs of (b) native yeasts and (c) yeast@PDA. (d–g) TEM micrographs of PDA-encapsulated yeast cells. (h) Growth curve of native and PDA-coated yeast cells. (i) Survival of native and coated yeast cells in the presence of lyticase. (Reprinted with permission from Ref. [83] Copyright 2011 American Chemical Society.)

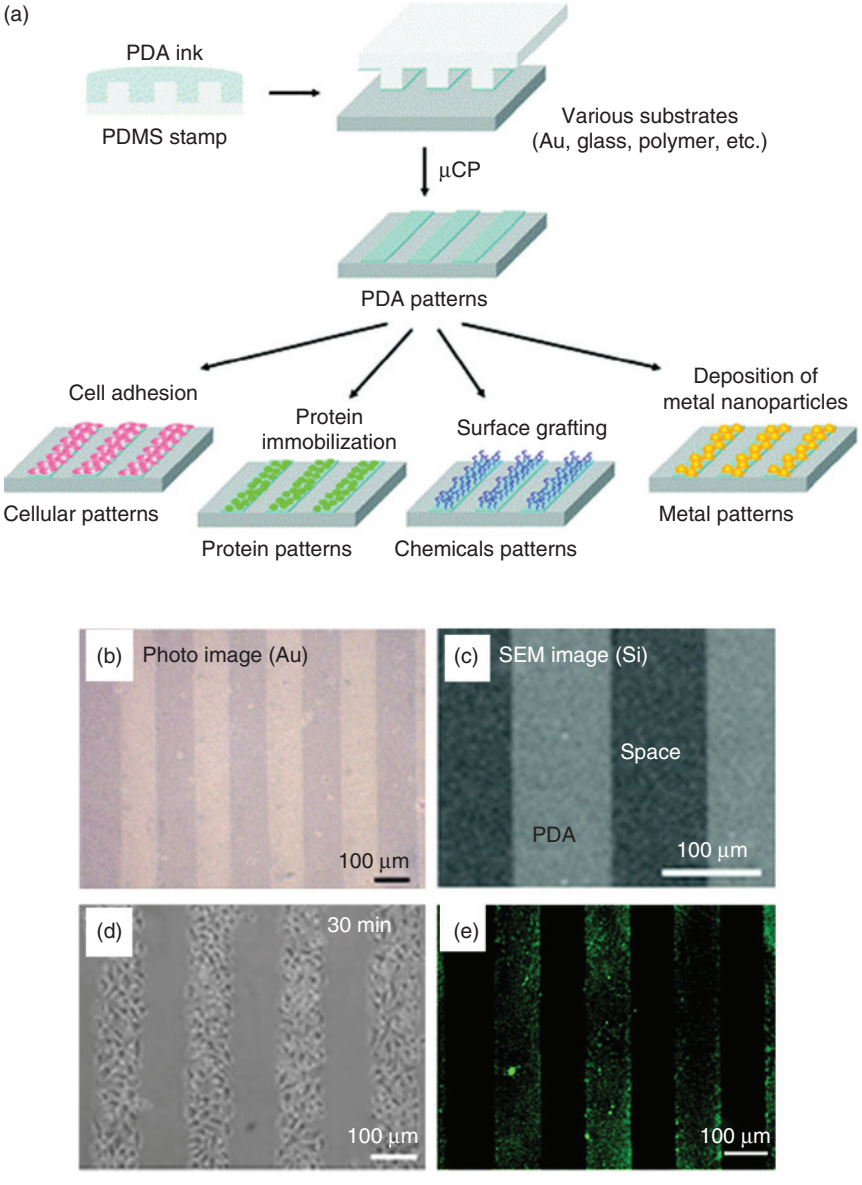

Figure 1.13 (a) Schematic representation of cell patterning with PDA as ink via micro-contact printing; (b) optical microscopic image of an imprinted PDA pattern on a gold substrate; (c) SEM images of PDA patterns on silicon; (d) SEM image of the cell-patterned substrate; (e) fluorescent microscopy image of the cell-patterned substrate after immobilization of fluorescein isothiocyanate conjugate – bovine serum albumin (FITC-BSA). (Reprinted with permission from Ref. [87] Copyright 2012 American Chemical Society.)

photon energy conversion into heat for cancer treatment [94–97]. In recent years, there has been a great deal of interest in new nanoparticles or therapeutic agents for cancer therapy. The PTT method has advantages in that it is highly specific and selective and can be used as a stimuli-responsive system, killing only those cells which are irradiated with NIR light and not affecting other normal cells [95]. However, the long term impact of these agents is still debatable which impedes clinical trials [98, 99]. Contrary to the commonly used nanoparticles, PDA has attracted great interest since PDA-coated Au nanorods have been reported as a good photothermal agent [100]. The strong absorption in the NIR region with the biocompatibility of PDA makes it an attractive material for PTT. Liu *et al*. reported the very first study on PDA colloidal particles for *in vivo* cancer therapy and it shows high photothermal conversion efficiency (Figure 1.14) [29]. PDA nanoparticles also display almost negligible toxicity for 4T1 cells even at high concentration, ~1.2 mg mL^{-1} (Figure 1.14). Coupled with exciting photothermal and excellent surface modification properties, PDA-based therapeutic agents should be a key material for PTT [101, 102].

Theranostics refers to the single approach of combined diagnostic and therapeutic capabilities. Recently, Lu and coworkers reported a PDA-nanocomposite-based theranostics system for dual-mode magnetic resonance imaging (MRI)

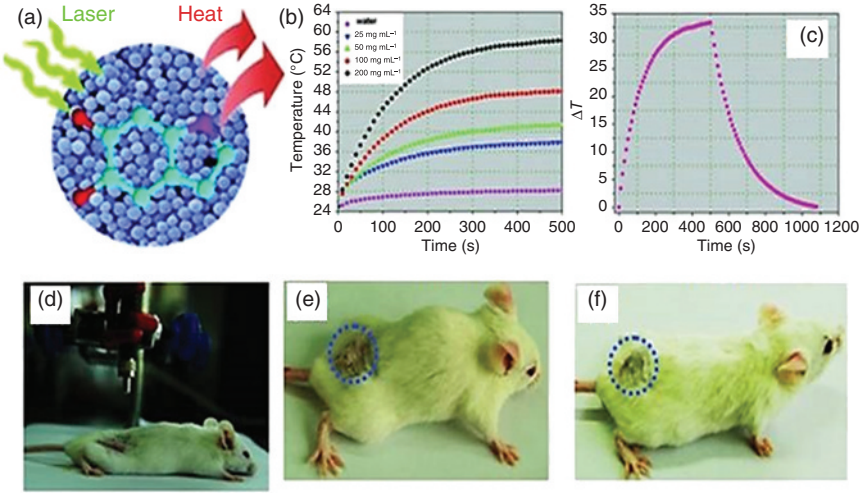

Figure 1.14 (a) Illustration of photothermal treatment (b) Time-dependent temperature change at different concentrations of PDA nanoparticle (NP) suspension. (c) The photothermal response of PDA NP suspension (200 μg mL^{-1}) for 500 s with an NIR laser (808 nm, 2 W cm^{-2}). (d–f) Digital photographs of the biocompatibility of PDA NPs with a tumor-bearing mouse for photothermal therapy. (g) A digital photograph of a 4T1 cell culture dish after incubation with PDA NPs and red circle shows the laser spot. (h–k) Confocal images of calcein acetoxymethyl (calcein AM) (green, live cells) and propidium iodide (red, dead cells) co-stained 4T1 cells after laser irradiation. (i) Cell viability of 4T1 cells after incubation with increasing concentrations of PDA NPs. (l) Cell viability of 4T1 cells treated with different concentrations of PDA NPs with laser irradiation (808 nm, 2 W cm^{-2}, 5 min). (Reprinted with permission from Ref. [29] Copyright 2013 Wiley-VCH.)

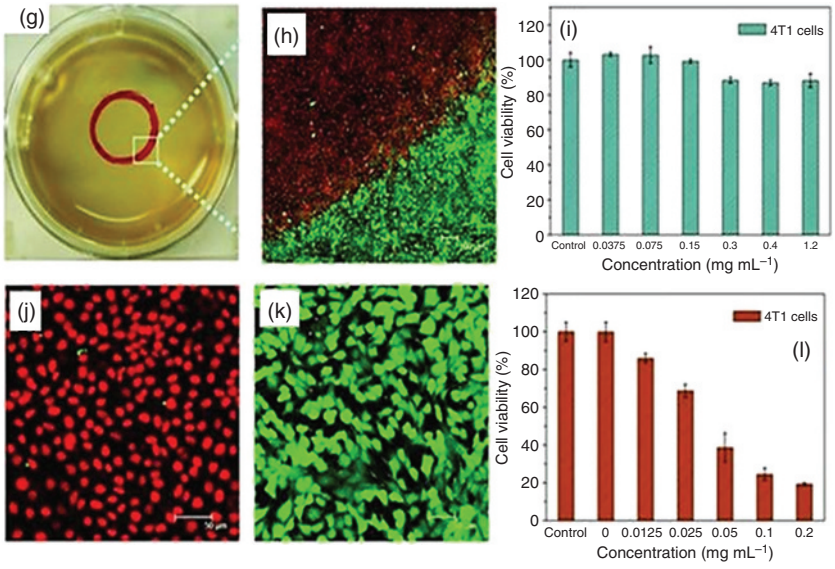

Figure 1.14 (*Continued*)

and shows the potential application in MRI-guided chemothermal treatment (Figure 1.15) [103]. Zhong *et al.* show PDA as a multifunctional nanocarrier for radioisotope therapy and cancer chemotherapy [104]. Thus, PDA has emerged as a potential material of choice for cancer therapy and diagnostic applications.

1.5 Conclusion and Future Prospectives

PDA, although only a few years old, has already attracted a great deal of attention and is becoming a potential candidate in the rapidly growing field of biomedical science. This chapter gives an overview of the synthesis protocols, characteristic properties, and the current state of the art of PDA material for biomedical applications. This exciting material has already shown a variety of interesting applications in very diverse fields such as biocompatible coatings, surface modification, cell adhesion, drug delivery, PTT, tissue engineering, and so on. Although considerable progress has been made, there are still some concerns about the PDA structure–property relationship; for instance, a definitive structural model, polymerization mechanism, is still not well established and continues to be debated. A combined experimental–computational strategy could be a method to solve this longstanding puzzle, which will be of great importance to both fundamental and biomedical applications. Resolving these issues will help take complete advantage of PDA in the biomedical field. Nevertheless, we believe that PDA will prove an emerging potential bioinspired material for biomedical science.

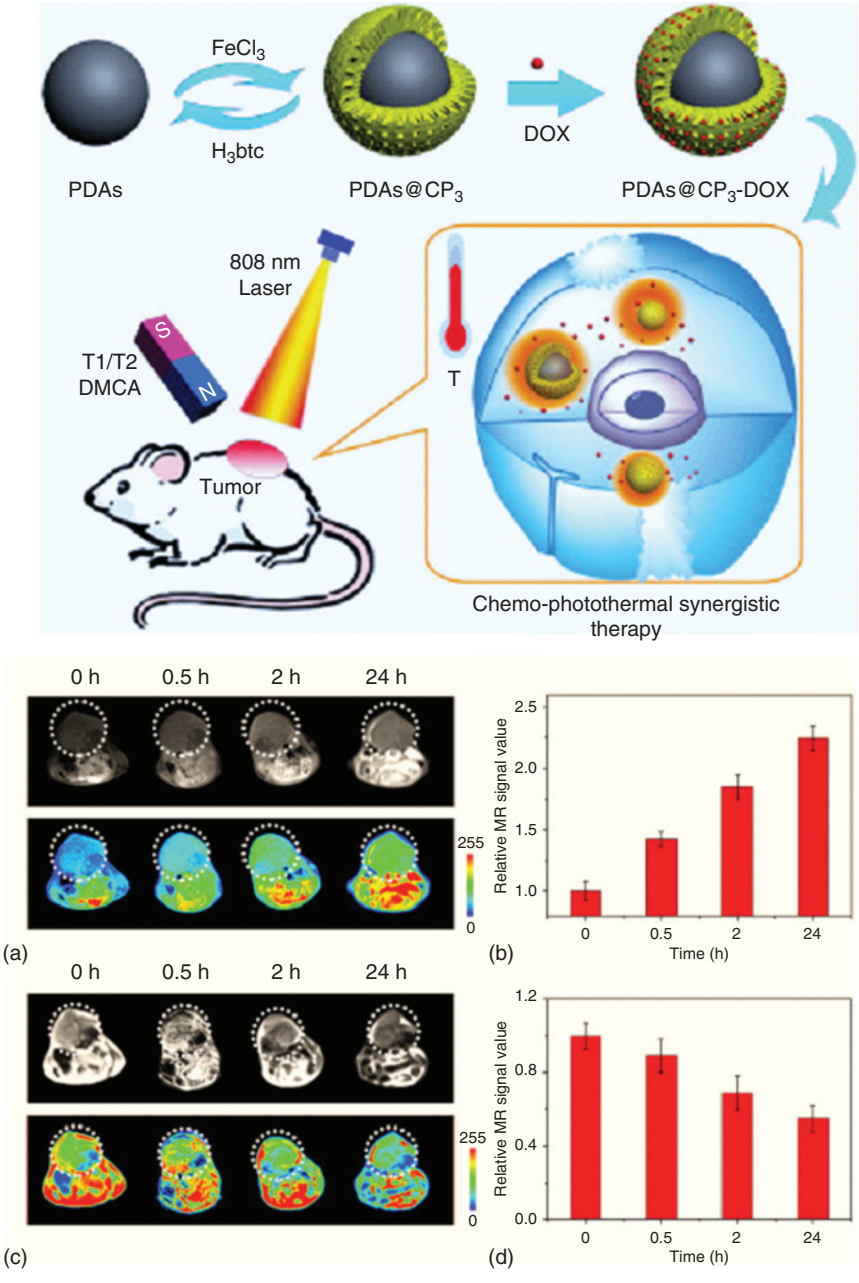

Figure 1.15 Schematic of the synthesis and application of PDAs@CP3-DOX. (a) *In vivo* T1, (c) T2; MR images of mice after intravenous injection of PDAs@CP3 at different time intervals, and its corresponding data analysis of T1 (b) and (d) T2-weighted MRI measurements. (Reprinted with permission from Ref. [103] Copyright 2015 Elsevier Ltd.)

References

1 Palivan, C.G., Goers, R., Najer, A., Zhang, X., Car, A., and Meier, W. (2016) Bioinspired polymer vesicles and membranes for biological and medical applications. *Chem. Soc. Rev.*, **45** (2), 377–411.

2 Sanchez, C., Arribart, H., and Giraud Guille, M.M. (2005) Biomimetism and bioinspiration as tools for the design of innovative materials and systems. *Nat. Mater.*, **4** (4), 277–288.

3 Liu, Y., Ai, K., and Lu, L. (2014) Polydopamine and its derivative materials: synthesis and promising applications in energy, environmental, and biomedical fields. *Chem. Rev.*, **114** (9), 5057–5115.

4 Lee, H., Dellatore, S.M., Miller, W.M., and Messersmith, P.B. (2007) Mussel-inspired surface chemistry for multifunctional coatings. *Science*, **318** (5849), 426–430.

5 Bernsmann, F., Ball, V., Addiego, F., Ponche, A., Michel, M., de Almeida Gracio, J.J., Toniazzo, V., and Ruch, D. (2011) Dopamine–melanin film deposition depends on the used oxidant and buffer solution. *Langmuir*, **27** (6), 2819–2825.

6 Łuczak, T. (2008) Preparation and characterization of the dopamine film electrochemically deposited on a gold template and its applications for dopamine sensing in aqueous solution. *Electrochim. Acta*, **53** (19), 5725–5731.

7 Dreyer, D.R., Miller, D.J., Freeman, B.D., Paul, D.R., and Bielawski, C.W. (2012) Elucidating the structure of poly(dopamine). *Langmuir*, **28** (15), 6428–6435.

8 Hong, S., Na, Y.S., Choi, S., Song, I.T., Kim, W.Y., and Lee, H. (2012) Non-covalent self-assembly and covalent polymerization co-contribute to polydopamine formation. *Adv. Funct. Mater.*, **22** (22), 4711–4717.

9 Della Vecchia, N.F., Avolio, R., Alfè, M., Errico, M.E., Napolitano, A., and d'Ischia, M. (2013) Building-block diversity in polydopamine underpins a multifunctional eumelanin-type platform tunable through a quinone control point. *Adv. Funct. Mater.*, **23** (10), 1331–1340.

10 Chen, C.-T., Chuang, C., Cao, J., Ball, V., Ruch, D., and Buehler, M.J. (2014) Excitonic effects from geometric order and disorder explain broadband optical absorption in eumelanin. *Nat. Commun.*, **5**, 3859.

11 Kobayashi, S. and Makino, A. (2009) Enzymatic polymer synthesis: an opportunity for green polymer chemistry. *Chem. Rev.*, **109** (11), 5288–5353.

12 Tan, Y., Deng, W., Li, Y., Huang, Z., Meng, Y., Xie, Q., Ma, M., and Yao, S. (2010) Polymeric bionanocomposite cast thin films with *in situ* laccase-catalyzed polymerization of dopamine for biosensing and biofuel cell applications. *J. Phys. Chem. B*, **114** (15), 5016–5024.

13 Ouyang, R., Lei, J., Ju, H., and Xue, Y. (2007) A molecularly imprinted copolymer designed for enantioselective recognition of glutamic acid. *Adv. Funct. Mater.*, **17** (16), 3223–3230.

14 Ai, K., Liu, Y., Ruan, C., Lu, L., and Lu, G. (2013) Sp^2 C-dominant N-doped carbon sub-micrometer spheres with a tunable size: a versatile platform for highly efficient oxygen-reduction catalysts. *Adv. Mater.*, **25** (7), 998–1003.

15 Jiang, X., Wang, Y., and Li, M. (2014) Selecting water–alcohol mixed solvent for synthesis of polydopamine nano-spheres using solubility parameter. *Sci. Rep.*, **4**, 6070.

16 Yan, D., Xu, P., Xiang, Q., Mou, H., Xu, J., Wen, W., Li, X., and Zhang, Y. (2016) Polydopamine nanotubes: bio-inspired synthesis, formaldehyde sensing properties and thermodynamic investigation. *J. Mater. Chem. A*, **4** (9), 3487–3493.

17 Xue, J., Zheng, W., Wang, L., and Jin, Z. (2016) Scalable fabrication of polydopamine nanotubes based on curcumin crystals. *ACS Biomater. Sci. Eng.*, **2** (4), 489–493.

18 Wu, T.-F. and Hong, J.-D. (2015) Dopamine–melanin nanofilms for biomimetic structural coloration. *Biomacromolecules*, **16** (2), 660–666.

19 Salomäki, M., Tupala, M., Parviainen, T., Leiro, J., Karonen, M., and Lukkari, J. (2016) Preparation of thin melanin-type films by surface-controlled oxidation. *Langmuir*, **32** (16), 4103–4411.

20 Yang, H.-C., Xu, W., Du, Y., Wu, J., and Xu, Z.-K. (2014) Composite free-standing films of polydopamine/polyethyleneimine grown at the air/water interface. *RSC Adv.*, **4** (85), 45415–45418.

21 Lynge, M.E., van der Westen, R., Postma, A., and Stadler, B. (2011) Polydopamine – a nature-inspired polymer coating for biomedical science. *Nanoscale*, **3** (1), 4916–4928.

22 Simon, J.D. and Peles, D.N. (2010) The red and the black. *Acc. Chem. Res.*, **43** (11), 1452–1460.

23 Barreto, W.J., Ponzoni, S., and Sassi, P. (1998) A Raman and UV–vis study of catecholamines oxidized with Mn(III). *Spectrochim. Acta, Part A*, **55** (1), 65–72.

24 Meredith, P. and Sarna, T. (2006) The physical and chemical properties of eumelanin. *Pigment Cell Res.*, **19** (6), 572–594.

25 McGinness, J., Corry, P., and Proctor, P. (1974) Amorphous semiconductor switching in melanins. *Science*, **183** (417), 853–855.

26 McGinness, J.E. (1972) Mobility gaps: a mechanism for band gaps in melanins. *Science*, **177** (4052), 896–897.

27 Coyne, K.J., Qin, X.-X., and Waite, J.H. (1997) Extensible collagen in mussel byssus: a natural block copolymer. *Science*, **277** (5333), 1830–1832.

28 Ooka, A.A. and Garrell, R.L. (2000) Surface-enhanced Raman spectroscopy of DOPA-containing peptides related to adhesive protein of marine mussel, *Mytilus edulis*. *Biopolymers*, **57** (2), 92–102.

29 Liu, Y., Ai, K., Liu, J., Deng, M., He, Y., and Lu, L. (2013) Dopamine–melanin colloidal nanospheres: an efficient near-infrared photothermal therapeutic agent for *in vivo* cancer therapy. *Adv. Mater.*, **25** (9), 1353–1359.

30 Pezzella, A., d'Ischia, M., Napolitano, A., Palumbo, A., and Prota, G. (1997) An integrated approach to the structure of Sepia melanin. Evidence for a high proportion of degraded 5,6-dihydroxyindole-2-carboxylic acid units in the pigment backbone. *Tetrahedron*, **53** (24), 8281–8286.

31 Bettinger, C.J., Bruggeman, J.P., Misra, A., Borenstein, J.T., and Langer, R. (2009) Biocompatibility of biodegradable semiconducting melanin films for nerve tissue engineering. *Biomaterials*, **30** (17), 3050–3057.

32 Lanzani, G. (2014) Materials for bioelectronics: organic electronics meets biology. *Nat. Mater.*, **13** (8), 775–776.

33 Green, R.A., Lovell, N.H., Wallace, G.G., and Poole-Warren, L.A. (2008) Conducting polymers for neural interfaces: challenges in developing an effective long-term implant. *Biomaterials*, **29** (24), 3393–3399.

34 Ghezzi, D., Antognazza, M.R., Dal Maschio, M., Lanzarini, E., Benfenati, F., and Lanzani, G. (2011) A hybrid bioorganic interface for neuronal photoactivation. *Nat. Commun.*, **2**, 166.

35 Simon, D.T., Gabrielsson, E.O., Tybrandt, K., and Berggren, M. (2016) Organic bioelectronics: bridging the signaling gap between biology and technology. *Chem. Rev.*, **116** (21), 13009–13041.

36 Rivnay, J., Leleux, P., Sessolo, M., Khodagholy, D., Hervé, T., Fiocchi, M., and Malliaras, G.G. (2013) Organic electrochemical transistors with maximum transconductance at zero gate bias. *Adv. Mater.*, **25** (48), 7010–7014.

37 Lin, P. and Yan, F. (2011) Organic thin-film transistors for chemical and biological sensing. *Adv. Mater.*, **24** (1), 34–51.

38 Gray-Schopfer, V., Wellbrock, C., and Marais, R. (2007) Melanoma biology and new targeted therapy. *Nature*, **445** (7130), 851–857.

39 Meredith, P., Powell, B.J., Riesz, J., Nighswander-Rempel, S.P., Pederson, M.R., and Moore, E.G. (2006) Towards structure–property–function relationships for eumelanin. *Soft Matter.*, **2** (1), 37–44.

40 Gonçalves, P., Baffa Filho, O., and Graeff, C. (2006) Effects of hydrogen on the electronic properties of synthetic melanin. *J. Appl. Phys.*, **99** (10), 104701.

41 Wünsche, J., Cicoira, F., Graeff, C.F., and Santato, C. (2013) Eumelanin thin films: solution-processing, growth, and charge transport properties. *J. Mater. Chem. B*, **1** (31), 3836–3842.

42 Jastrzebska, M.M., Isotalo, H., Paloheimo, J., and Stubb, H. (1996) Electrical conductivity of synthetic DOPA-melanin polymer for different hydration states and temperatures. *J. Biomater. Sci., Polym. Ed.*, **7** (7), 577–586.

43 Mostert, A., Meredith, P., Powell, B., and Gentle, I. (2016) Understanding melanin: a nano-based material for the future, in Nanomaterials: Science and Applications, Pan Stanford, Boca Raton, FL, pp. 175–202.

44 Abbas, M., D'Amico, F., Morresi, L., Pinto, N., Ficcadenti, M., Natali, R., Ottaviano, L., Passacantando, M., Cuccioloni, M., and Angeletti, M. (2009) Structural, electrical, electronic and optical properties of melanin films. *Eur. Phys. J.*, **28** (3), 285–291.

45 Culp, C., Eckels, D., and Sidles, P. (1975) Threshold switching in melanin. *J. Appl. Phys.*, **46** (8), 3658–3660.

46 Filatovs, J., McGinness, J., and Corry, P. (1976) Thermal and electronic contributions to switching in melanins. *Biopolymers*, **15** (11), 2309–2312.

47 Mostert, A.B., Davy, K.J., Ruggles, J.L., Powell, B.J., Gentle, I.R., and Meredith, P. (2010) Gaseous adsorption in melanins: hydrophilic biomacromolecules with high electrical conductivities. *Langmuir*, **26** (1), 412–416.

48 Mostert, A.B., Powell, B.J., Gentle, I.R., and Meredith, P. (2012) On the origin of electrical conductivity in the bio-electronic material melanin. *Appl. Phys. Lett.*, **100** (9), 093701.

49 Tran, M.L., Powell, B.J., and Meredith, P. (2006) Chemical and structural disorder in eumelanins: a possible explanation for broadband absorbance. *Biophys. J.*, **90** (3), 743–752.

50 Powell, M.R. and Rosenberg, B. (1970) The nature of the charge carriers in solvated biomacromolecules. *J. Bioenerg. Biomembr.*, **1** (6), 493–509.

51 Blundell, S. (1999) Spin-polarized muons in condensed matter physics. *Contemp. Phys.*, **40** (3), 175–192.

52 Pratt, F. (2004) Muon spin relaxation as a probe of electron motion in conducting polymers. *J. Phys. Condens. Matter*, **16** (40), S4779.

53 Roduner, E. (1991) Radical reorientation dynamics studied by positive-muon avoided level crossing resonance. *Hyperfine Interact.*, **65** (1–4), 857–871.

54 Mostert, A.B., Powell, B.J., Pratt, F.L., Hanson, G.R., Sarna, T., Gentle, I.R., and Meredith, P. (2012) Role of semiconductivity and ion transport in the electrical conduction of melanin. *Proc. Natl. Acad. Sci. U.S.A.*, **109** (23), 8943–8947.

55 Mostert, A.B., Hanson, G.R., Sarna, T., Gentle, I.R., Powell, B.J., and Meredith, P. (2013) Hydration-controlled X-band EPR spectroscopy: a tool for unravelling the complexities of the solid-state free radical in eumelanin. *J. Phys. Chem. B*, **117** (17), 4965–4972.

56 Khan, Z., Khannam, M., Vinothkumar, N., De, M., and Qureshi, M. (2012) Hierarchical 3D NiO–CdS heteroarchitecture for efficient visible light photocatalytic hydrogen generation. *J. Mater. Chem.*, **22** (24), 1090–1095.

57 Khan, Z., Chetia, T.R., and Qureshi, M. (2012) Rational design of hyperbranched 3D heteroarrays of SrS/CdS: synthesis, characterization and evaluation of photocatalytic properties for efficient hydrogen generation and organic dye degradation. *Nanoscale*, **4** (11), 3543–3550.

58 Ansari, S.A., Khan, Z., Ansari, M.O., and Cho, M.H. (2016) Earth-abundant stable elemental semiconductor red phosphorus-based hybrids for environmental remediation and energy storage applications. *RSC Adv.*, **6** (50), 44616–44629.

59 Khan, Z., Chetia, T.R., Vardhaman, A.K., Barpuzary, D., Sastri, C.V., and Qureshi, M. (2012) Visible light assisted photocatalytic hydrogen generation and organic dye degradation by CdS–metal oxide hybrids in presence of graphene oxide. *RSC Adv.*, **2** (32), 12122–12128.

60 Barpuzary, D., Khan, Z., Vinothkumar, N., De, M., and Qureshi, M. (2012) Hierarchically grown urchinlike CdS@ZnO and CdS@Al_2O_3 heteroarrays for efficient visible-light-driven photocatalytic hydrogen generation. *J. Phys. Chem. C*, **116** (1), 150–156.

61 Feng, J.-J., Zhang, P.-P., Wang, A.-J., Liao, Q.-C., Xi, J.-L., and Chen, J.-R. (2012) One-step synthesis of monodisperse polydopamine-coated silver core–shell nanostructures for enhanced photocatalysis. *New J. Chem.*, **36** (1), 148–154.

62 Mao, W.-X., Lin, X.-J., Zhang, W., Chi, Z.-X., Lyu, R.-W., Cao, A.-M., and Wan, L.-J. (2016) Core–shell structured TiO_2@polydopamine for highly active visible-light photocatalysis. *Chem. Commun.*, **52** (44), 7122–7125.

63 Ang, J.M., Du, Y., Tay, B.Y., Zhao, C., Kong, J., Stubbs, L.P., and Lu, X. (2016) One-pot synthesis of Fe(III)–polydopamine complex nanospheres: morphological evolution, mechanism, and application of the carbonized hybrid nanospheres in catalysis and Zn–air battery. *Langmuir*, **32** (36), 9265–9275.

64 Jiang, H., Yang, L., Li, C., Yan, C., Lee, P.S., and Ma, J. (2011) High-rate electrochemical capacitors from highly graphitic carbon-tipped manganese oxide/mesoporous carbon/manganese oxide hybrid nanowires. *Energy Environ. Sci.*, **4** (5), 1813–1819.

65 Nam, H.J., Kim, B., Ko, M.J., Jin, M., Kim, J.M., and Jung, D.-Y. (2012) A new mussel-inspired polydopamine sensitizer for dye-sensitized solar cells: controlled synthesis and charge transfer. *Chem. Eur. J.*, **18** (44), 14000–14007.

66 Yu, B., Wang, D.A., Ye, Q., Zhou, F., and Liu, W. (2009) Robust polydopamine nano/microcapsules and their loading and release behavior. *Chem. Commun.*, (44), 6789–6791.

67 Zhang, L., Shi, J., Jiang, Z., Jiang, Y., Meng, R., Zhu, Y., Liang, Y., and Zheng, Y. (2011) Facile preparation of robust microcapsules by manipulating metal-coordination interaction between biomineral layer and bioadhesive layer. *ACS Appl. Mater. Interfaces*, **3** (2), 597–605.

68 Zhang, L., Shi, J., Jiang, Z., Jiang, Y., Qiao, S., Li, J., Wang, R., Meng, R., Zhu, Y., and Zheng, Y. (2011) Bioinspired preparation of polydopamine microcapsule for multienzyme system construction. *Green Chem.*, **13** (2), 300–306.

69 Cui, J., Wang, Y., Postma, A., Hao, J., Hosta-Rigau, L., and Caruso, F. (2010) Monodisperse polymer capsules: tailoring size, shell thickness, and hydrophobic cargo loading via emulsion templating. *Adv. Funct. Mater.*, **20** (10), 1625–1631.

70 Liu, Q., Yu, B., Ye, W., and Zhou, F. (2011) Highly selective uptake and release of charged molecules by pH-responsive polydopamine microcapsules. *Macromol. Biosci.*, **11** (9), 1227–1234.

71 Dalby, M.J., Gadegaard, N., Tare, R., Andar, A., Riehle, M.O., Herzyk, P., Wilkinson, C.D.W., and Oreffo, R.O.C. (2007) The control of human mesenchymal cell differentiation using nanoscale symmetry and disorder. *Nat. Mater.*, **6** (1), 997–1003.

72 Wu, C., Fan, W., Chang, J., and Xiao, Y. (2011) Mussel-inspired porous SiO_2 scaffolds with improved mineralization and cytocompatibility for drug delivery and bone tissue engineering. *J. Mater. Chem.*, **21** (45), 18300–18307.

73 Ku, S.H. and Park, C.B. (2010) Human endothelial cell growth on mussel-inspired nanofiber scaffold for vascular tissue engineering. *Biomaterials*, **31** (36), 9431–9437.

74 Xu, H., Shi, X., Ma, H., Lv, Y., Zhang, L., and Mao, Z. (2011) The preparation and antibacterial effects of dopa-cotton/AgNPs. *Appl. Surf. Sci.*, **257** (15), 6799–6803.

75 Sileika, T.S., Kim, H.-D., Maniak, P., and Messersmith, P.B. (2011) Antibacterial performance of polydopamine-modified polymer surfaces containing passive and active components. *ACS Appl. Mater. Interfaces*, **3** (1), 4602–4610.

76 Ding, X., Yang, C., Lim, T.P., Hsu, L.Y., Engler, A.C., Hedrick, J.L., and Yang, Y.-Y. (2012) Antibacterial and antifouling catheter coatings using surface grafted PEG-*b*-cationic polycarbonate diblock copolymers. *Biomaterials*, **33** (28), 6593–6603.

77 Wolfbeis, O.S. (2015) An overview of nanoparticles commonly used in fluorescent bioimaging. *Chem. Soc. Rev.*, **44** (14), 4743–4768.

78 Jaiswal, A., Ghosh, S.S., and Chattopadhyay, A. (2012) One step synthesis of C-dots by microwave mediated caramelization of poly(ethylene glycol). *Chem. Commun.*, **48** (3), 407–409.

79 Zhang, Y., Bai, Y., Jia, J., Gao, N., Li, Y., Zhang, R., Jiang, G., and Yan, B. (2014) Perturbation of physiological systems by nanoparticles. *Chem. Soc. Rev.*, **43** (10), 3762–3809.

80 Zhang, X., Wang, S., Xu, L., Feng, L., Ji, Y., Tao, L., Li, S., and Wei, Y. (2012) Biocompatible polydopamine fluorescent organic nanoparticles: facile preparation and cell imaging. *Nanoscale*, **4** (18), 5581–5584.

81 Nurunnabi, M., Khatun, Z., Nafiujjaman, M., Lee, D.-G., and Lee, Y.-K. (2013) Surface coating of graphene quantum dots using mussel-inspired polydopamine for biomedical optical imaging. *ACS Appl. Mater. Interfaces*, **5** (16), 8246–8253.

82 Zhang, P.-H., Cao, J.-T., Min, Q.-H., and Zhu, J.-J. (2013) Multi-shell structured fluorescent–magnetic nanoprobe for target cell imaging and on-chip sorting. *ACS Appl. Mater. Interfaces*, **5** (15), 7417–7424.

83 Yang, S.H., Kang, S.M., Lee, K.-B., Chung, T.D., Lee, H., and Choi, I.S. (2011) Mussel-inspired encapsulation and functionalization of individual yeast cells. *J. Am. Chem. Soc.*, **133** (9), 2795–2797.

84 Ku, S.H., Ryu, J., Hong, S.K., Lee, H., and Park, C.B. (2010) General functionalization route for cell adhesion on non-wetting surfaces. *Biomaterials*, **31** (9), 2535–2541.

85 Tsai, W.-B., Chen, W.-T., Chien, H.-W., Kuo, W.-H., and Wang, M.-J. (2011) Poly(dopamine) coating of scaffolds for articular cartilage tissue engineering. *Acta Biomater.*, **7** (1), 4187–4194.

86 Ku, S.H. and Park, C.B. (2013) Combined effect of mussel-inspired surface modification and topographical cues on the behavior of skeletal myoblasts. *Adv. Healthc. Mater.*, **2** (11), 1445–1450.

87 Chien, H.-W., Kuo, W.-H., Wang, M.-J., Tsai, S.-W., and Tsai, W.-B. (2012) Tunable micropatterned substrates based on poly(dopamine) deposition via microcontact printing. *Langmuir*, **28** (13), 5775–5782.

88 Ku, S.H., Lee, J.S., and Park, C.B. (2010) Spatial control of cell adhesion and patterning through mussel-inspired surface modification by polydopamine. *Langmuir*, **26** (19), 15104–15108.

89 Wang, P.Y., Wu, T.H., Chao, P.H.G., Kuo, W.H., Wang, M.J., Hsu, C.C., and Tsai, W.B. (2013) Modulation of cell attachment and collagen production of anterior cruciate ligament cells via submicron grooves/ridges structures with different cell affinity. *Biotechnol. Bioeng.*, **110** (1), 327–337.

90 Zhong, S., Luo, R., Wang, X., Tang, L., Wu, J., Wang, J., Huang, R., Sun, H., and Huang, N. (2014) Effects of polydopamine functionalized titanium dioxide nanotubes on endothelial cell and smooth muscle cell. *Colloids Surf., B*, **116**, 553–560.

91 Yang, Z., Tu, Q., Zhu, Y., Luo, R., Li, X., Xie, Y., Maitz, M.F., Wang, J., and Huang, N. (2012) Mussel-inspired coating of polydopamine directs endothelial and smooth muscle cell fate for re-endothelialization of vascular devices. *Adv. Healthc. Mater.*, **1** (5), 548–559.

92 Luo, R., Tang, L., Zhong, S., Yang, Z., Wang, J., Weng, Y., Tu, Q., Jiang, C., and Huang, N. (2013) *In vitro* investigation of enhanced hemocompatibility and endothelial cell proliferation associated with quinone-rich polydopamine coating. *ACS Appl. Mater. Interfaces*, **5** (5), 1704–1714.

93 Ding, Y., Yang, Z., Bi, C.W., Yang, M., Zhang, J., Xu, S.L., Lu, X., Huang, N., Huang, P., and Leng, Y. (2014) Modulation of protein adsorption, vascular cell selectivity and platelet adhesion by mussel-inspired surface functionalization. *J. Mater. Chem. B*, **2** (24), 3819–3829.

94 Hirsch, L.R., Stafford, R., Bankson, J., Sershen, S., Rivera, B., Price, R., Hazle, J., Halas, N.J., and West, J. (2003) Nanoshell-mediated near-infrared thermal therapy of tumors under magnetic resonance guidance. *Proc. Natl. Acad. Sci. U.S.A.*, **100** (23), 13549–13554.

95 Abadeer, N.S. and Murphy, C.J. (2016) Recent progress in cancer thermal therapy using gold nanoparticles. *J. Phys. Chem. C*, **10** (9), 4691–4716.

96 Huang, X., El-Sayed, I.H., Qian, W., and El-Sayed, M.A. (2006) Cancer cell imaging and photothermal therapy in the near-infrared region by using gold nanorods. *J. Am. Chem. Soc.*, **18** (6), 2115–2210.

97 Kuo, W.S., Chang, C.N., Chang, Y.T., Yang, M.H., Chien, Y.H., Chen, S.J., and Yeh, C.S. (2010) Gold nanorods in photodynamic therapy, as hyperthermia agents, and in near-infrared optical imaging. *Angew. Chem. Int. Ed.*, **1** (15), 2771–2775.

98 Nel, A., Xia, T., Mädler, L., and Li, N. (2006) Toxic potential of materials at the nanolevel. *Science*, **311** (5761), 622–627.

99 Sharifi, S., Behzadi, S., Laurent, S., Forrest, M.L., Stroeve, P., and Mahmoudi, M. (2012) Toxicity of nanomaterials. *Chem. Soc. Rev.*, **41** (6), 2323–2343.

100 Black, K.C., Yi, J., Rivera, J.G., Zelasko-Leon, D.C., and Messersmith, P.B. (2013) Polydopamine-enabled surface functionalization of gold nanorods for cancer cell-targeted imaging and photothermal therapy. *Nanomedicine*, **8** (1), 17–28.

101 Zhang, R., Su, S., Hu, K., Shao, L., Deng, X., Sheng, W., and Wu, Y. (2015) Smart micelle@polydopamine core–shell nanoparticles for highly effective chemo–photothermal combination therapy. *Nanoscale*, **7** (46), 19722–19731.

102 Wu, M., Zhang, D., Zeng, Y., Wu, L., Liu, X., and Liu, J. (2015) Nanocluster of superparamagnetic iron oxide nanoparticles coated with poly(dopamine) for magnetic field-targeting, highly sensitive MRI and photothermal cancer therapy. *Nanotechnology*, **26** (11), 115102.

103 Chen, Y., Ai, K., Liu, J., Ren, X., Jiang, C., and Lu, L. (2016) Polydopamine-based coordination nanocomplex for T1/T2 dual mode magnetic resonance imaging-guided chemo-photothermal synergistic therapy. *Biomaterials*, **77**, 198–206.

104 Zhong, X., Yang, K., Dong, Z., Yi, X., Wang, Y., Ge, C., Zhao, Y., and Liu, Z. (2015) Polydopamine as a biocompatible multifunctional nanocarrier for combined radioisotope therapy and chemotherapy of cancer. *Adv. Funct. Mater.*, **25** (47), 7327–7336.